

The X-ray Warm Absorber in NGC3516

Smita Mathur¹

smita@cfa.harvard.edu

Belinda J. Wilkes¹

belinda@cfa.harvard.edu

Thomas Aldcroft¹

taldcroft@cfa.harvard.edu

Abstract

The Seyfert 1 galaxy, NGC3516 has been the subject of many absorption line studies at both ultraviolet and X-ray wavelengths. In the UV, strong, broad, variable associated metal line absorption with velocity width $\sim 2000 \text{ km s}^{-1}$ is thought to originate in gas with $N_{\text{H}} \gtrsim 10^{19} \text{ cm}^{-2}$ lying between 0.01 and 9 pc from the central active nucleus. The *Ginga* X-ray data are consistent with several possibilities: a warm absorber and a cold absorber combined either with partial covering or an unusually strong reflection spectrum. We present ROSAT observations of NGC3516 which show a strong detection of a warm absorber dominated by a blend of OVII/OVIII edges at $\sim 0.8 \text{ keV}$ with $N_{\text{H}} \sim 7 \times 10^{21} \text{ cm}^{-2}$ and U: 8–12. We argue that NGC3516 contains an outflowing ‘XUV’ absorber showing the presence of X-ray absorption edges, that are consistent with the presence of broad absorption lines in the old IUE spectra and their disappearance in the new UV observations. Our dynamical model suggests that the OVII absorption edge will continue to weaken compared to the OVIII edge, an easily testable prediction with future missions like AXAF. Eventually the source would be transparent to the X-rays unless a new absorption system is produced.

¹Harvard-Smithsonian Center for Astrophysics, 60 Garden St., Cambridge, MA 02138

1. Introduction

Given the recent success of efforts to unify associated ultraviolet (UV) metal line absorbers with ionized (“warm”) absorbers seen in the X-ray (Mathur *et al.* 1994, 1995, Mathur 1994), NGC3516 is a prime candidate for such an investigation. NGC 3516 is a low-redshift ($z=0.0089$) Seyfert 1 galaxy with a variable, associated UV absorption line system which has been extensively monitored with IUE (Voit et al 1987, Walter et al 1990, Kolman *et al.* 1993 (KEA); Koratkar *et al.* 1996). Based on IUE spectra, NGC 3516 contains the strongest (largest equivalent width) UV absorption system known in a Seyfert 1 galaxy. This system contains at least two distinct components: a broad (FWHM \sim 2000 km s $^{-1}$) variable component, most likely to be associated with the X-ray absorber, and a narrow (\sim 500 km s $^{-1}$) non-variable component. The equivalent-width of the CIV λ 1549 broad+narrow absorption line varies by a factor of 4-5 and anti-correlates with the UV continuum level on short timescales of days. Walter *et al.* (1990) have also found variations on longer timescales (\sim years) possibly due to the absorbing cloud passing through the line of sight. Recent observations have found that the broad variable absorption lines of CIV and NV have disappeared (Koratkar *et al.* 1996, Kriss *et al.* 1996b).

The X-ray absorber is not so well-known or heavily studied. The highest quality data to date are from 1989 *Ginga* observations reported by KEA, consistent with several possibilities: a warm absorber, a cold absorber with partial covering, or a cold absorber with an unusually strong reflection spectrum. If the absorption is due to the cold matter, the column density is large $N_H \sim 10^{22}$ cm $^{-2}$. These authors concluded that a common origin for the X-ray and UV absorbing material is not possible due to the apparently different ionization states and column densities of the UV and X-ray absorbers. *Ginga* data were later re-analyzed by Nandra & Pounds (1994), showing that a warm absorber describes the data well. New ASCA observations of NGC3516 are presented in a recent preprint by Kriss *et al.* (1996a), which show a presence of an ionized absorber similar to the one discussed in this paper.

Here we present a long (\sim 1 day) high signal-to-noise ROSAT (Trumper 1983) Position Sensitive Proportional Counter (PSPC, Pfefferman et al. 1987) spectrum of NGC3516 obtained in 1992 which, with its lower energy range, is sensitive to absorption edges due to ionized oxygen. The high S/N allows the strong detection of both OVII and OVIII edges independently, in spite of the limited spectral resolution of the PSPC. These edges show the presence of an ionized absorber in X-rays. We discuss the constraints these data place on the physical conditions in the absorber and revisit the question of a common origin for

the X-ray and UV absorbing material.

2. *ROSAT* Observations and Data Analysis

NGC 3516 was observed with the *ROSAT* PSPC on October 1, 1992 for a total livetime of 13,081 sec. over a real time span of 83,455 sec. We retrieved the data from the HEASARC² database and analyzed it using the PROS³ package in IRAF. The source counts were extracted from within a 3' radius circle centered on the source centroid. The small background was estimated from an annulus centered on the source and inner and outer radii of 5' and 7' respectively. The total net counts were $59,225 \pm 246$ yielding a count rate of $4.53 \pm 0.02 \text{ s}^{-1}$ (Table 1) (c.f. 1420 ± 340 counts for 3C351 in which absorption edges were detected, Fiore et al. 1993).

Since NGC 3516 is known to be a variable X-ray source (Halpern 1982), we looked for X-ray flux variations over the total span of the observation. A total of eight good time intervals (GTI) were found. The net counts in each GTI were extracted in the same way as discussed above. The live time, count rate and the total counts in each GTI are given in Table 1. The change in count rate shows the flux variability which is clearly seen in the light curve in Figure 1. The variations are significant at the 99.99% level (χ^2 test, K-S test using PROS task “vartst”). Since variability of $\sim 40\%$ is clearly seen, the source spectrum for each GTI was extracted separately, and analyzed using XSPEC⁴. As can be seen in Table 1, the individual GTIs contain sufficient counts to fit complex spectra.

2.1. Spectral Analysis

The results of the spectral analysis of all the datasets are presented in Table 2. All the spectral fits were made to the 3–34 PHA channels as extracted by the standard PROS

²High Energy Astrophysics Science Archive Research Center is a service of the Laboratory for High Energy Astrophysics (LHEA) at NASA/GSFC.

³Post-Reduction Offline Software

⁴X-ray SPECTral analysis software available from NASA-GSFC

analysis. Channels 1 and 2 were ignored since they are inadequately calibrated. The response matrix released in January 1993 was employed. The errors represent the 90% confidence interval.

Our first fit used a simple power law with absorption by cold material at zero redshift with solar abundances, and cross sections by Morrison and McCammon (1983). Both the power-law slope and absorption column density were free to vary. In all GTIs, the column density of the cold absorber (N_H) was consistent (within 90% confidence) with the Galactic value of 3×10^{20} atoms cm^{-2} (Heiles 1975) (e.g. $N_H = 3.0 \pm 0.1 \times 10^{20}$ cm^{-2} in GTI 4; and $N_H = 2.4 \pm 0.5 \times 10^{20}$ cm^{-2} in GTI 7). The single power-law (and all subsequent) fits were redone with N_H fixed at the Galactic value and the results are presented in Table 2.

The single power-law fits are unacceptably bad, with $\chi^2_\nu \gtrsim 4$ and significant negative residuals between 0.7 and 1 keV (see Figure 2). This is a clear signature of K-shell absorption edges due to OVII and/or OVIII. We then fitted the spectra with a power-law (PL), cold Galactic absorption, and an edge at the energy of a redshifted OVII K-edge ($E(\text{rest frame})=0.74$ keV, $z=0.0089$). The improvement in the fit was dramatic, as demonstrated by the results of an F-test (Table 2), although small residuals remained near the edge in several GTIs. For consistency we then fitted the spectrum of all GTIs with an additional edge at the energy of the redshifted OVIII K-edge ($E(\text{rest frame})=0.87$ keV). Once again the improvement in the fit was significant and the spectrum was well fit ($\chi^2_\nu = 1.1$, Table 2, Figure 3) except for GTI 4 ($\chi^2_\nu = 1.6$, see below). Thus, even though the energy resolution of the ROSAT PSPC is insufficient to resolve the OVII/OVIII edges, the absorption in NGC 3516 is so strong ($\tau \sim 1$) that the data *require* two separate edges in half of the GTIs (> 99% confidence, labeled “c” in Table 2). These are not simply the four GTIs with highest S/N.

As discussed above, the data were consistent with $N_H=N_H(\text{Galactic})$. To confirm that this is the case even with the ‘power-law plus two edges’ model, we fit the spectra with a PL, Galactic N_H (fixed), two edges and an additional cold N_H at the source. The fitted value of the additional column density was always much smaller than Galactic (e.g. 1.2×10^{18} atoms cm^{-2} for GTI 1) and consistent with zero. Excess N_H is clearly not required. GTI 4 was the only exception for which an excess absorption $N_H = 4.9 \pm 2.6 \times 10^{19}$ improved the fit significantly ($\chi^2_\nu = 1.28$, improvement > 99% significant, F-test). Parameters for this best fit model are given in the last line for GTI 4 in Table 2. Since GTI 4 has the maximum S/N, it is possible that a small additional column is present ($N_H \lesssim 3.7 \times 10^{19}$ cm^{-2}) but undetected in the remaining GTIs.

Since the flux is found to be variable but the absorption and spectral shapes are not (see section 3.1), we also fitted all the GTIs together with a ‘power-law plus two edges’ model allowing their normalizations to be free (Table 2). Excess absorption was not required, though the best value was $N_H = 3.3_{-3.3}^{+1.3} \times 10^{19} \text{ cm}^{-2}$, similar to the results above.

3. The X-ray warm absorber

Knowing the total column density and the opacity of the oxygen edges, we can constrain the ionization state of the warm absorber (Mathur, Elvis & Wilkes, 1995). The present case of NGC3516 is a little tricky, however, because N_H is not known. Instead we need to estimate the N_H and the ionization parameter (U) by fitting the spectrum with a warm absorber model. Alternatively we can derive these parameters in a more elegant way, exploiting the fact that we observe *both* OVII and OVIII edges in NGC3516. We apply both these methods below.

Let τ_{OVII} and τ_{OVIII} be the opacities due to K-edges of OVII and OVIII respectively. The absorption cross-sections of OVII and OVIII are $0.28 \times 10^{-18} \text{ cm}^{-2}$ and $0.098 \times 10^{-18} \text{ cm}^{-2}$ respectively (CLOUDY; Ferland 1991). Using these we can derive the column densities of the two ions, N_{OVII} and N_{OVIII} and the ratio $N_{OVII}/N_{OVIII} = f_{OVII}/f_{OVIII}$ where f_{OVII} and f_{OVIII} represent the fraction of oxygen in these two stages of ionization. Over the span of ROSAT observations (GTI 1 through 8), f_{OVII}/f_{OVIII} ranges from ~ 0.16 to 5.8. We determined the dependence of f_{OVII} and f_{OVIII} on the ionization parameter, U , for a photoionized gas cloud using CLOUDY and assuming solar abundances and a standard AGN continuum (Ferland 1991, version 80.06). The density was assumed to be 10^5 cm^{-3} . The results are displayed in Figure 4 and demonstrate that the observed range in f_{OVII}/f_{OVIII} occupies a small area in the parameter space of fractional ionization as a function of ionization parameter. Using Figure 4, we can not only infer the ionization parameter (U ranges from ~ 3.2 at GTI 6 to ~ 18 at GTI 3), but also f_{OVII} and f_{OVIII} . These lie in the range $0.06 < f_{OVII} < 0.8$, and $0.1 < f_{OVIII} < 0.5$. Using the abundance of oxygen relative to hydrogen (8.51×10^{-4} ; Grevesse & Andres 1989) and f_{OVII} or f_{OVIII} , the total column density is readily calculated to be $N_H = 0.4 - 2.2 \times 10^{22} \text{ cm}^{-2}$.

As discussed above, the ionization parameter of the X-ray absorber is determined using Figure 4. It should be noted however that the exact relation of ionization fractions and U depends upon the shape of the input continuum (Fiore *et al.* 1993, Mathur *et al.* 1994). We

have used a standard AGN continuum (CLOUDY, Ferland 1991) in our analysis. With a different continuum shape, the inferred range of U would change but, qualitatively, Figure 4 would remain the same. For example, an X-ray slope of 1.0 (as seen in the ROSAT data) rather than the 0.7 assumed in the standard continuum leads to a larger value of U : $8.5 \lesssim U \lesssim 23$. On the other hand if the X-ray slope is much flatter ($\alpha \sim 0.3$) as seen by *Ginga*, U would be correspondingly lower. Independently of the shape of the input continuum, the X-ray data for the absorber in NGC3516 requires $f_{\text{OVII}}/f_{\text{OVIII}} \sim 1$, corresponding to a highly ionized absorber. A similar result was obtained by Kriss *et al.* (1996a) who used a variety of incident continua and found that their results were independent of the exact shape of the continuum apart from the deduced ionization parameter U . The only derived quantity that depends upon the exact value of U (and so on the shape of the continuum) is the distance of the absorber from the central continuum source ($R^2 = Q/4\pi U n c$). Since there is a four orders of magnitude uncertainty in density, n (section 3.1), the uncertainty in R is very large, far exceeding that due to the uncertainty in U . We will thus assume the standard continuum in the rest of the paper. Kriss *et al.* (1996a) use a continuum with significantly flatter α_{ox} and correspondingly lower value of $U=1.66$ in their analysis of 1995 ASCA data, so we cannot directly compare our U value with Kriss *et al.* (1996a).

Unlike the other objects showing an X-ray warm absorber (e.g. 3C351: Fiore *et al.* 1993, NGC3783: Turner *et al.* 1994, NGC5548: Mathur *et al.* 1995), the X-ray continuum in NGC3516 is transparent at low energies. To investigate this absence of a low energy turnover in the ROSAT spectrum of NGC3516, we generated the transmitted spectrum for the best fit U and N_H (using CLOUDY). Figure 5 shows the input spectrum (solid line; “standard” AGN spectrum) and the transmitted spectrum (dotted line) over the ROSAT and *Ginga* energy bands. It is clearly seen that the spectrum is transparent at low energies and the OVII/OVIII absorption edges are prominent in the ROSAT energy range.

As a consistency check we also fitted the spectra with a warm absorber model. The models were generated using CLOUDY and then incorporated into XSPEC as ‘table models’. The input parameters to CLOUDY were same as used above. The results of the fits are given in Table 3 and are consistent with the results discussed above. When N_H is fixed to the Galactic value, the fits are acceptable for all the GTIs except GTI 4, similar to the results in section 2.1 (first line for each GTI in Table 3). When N_H was allowed to be free, the fits improved and were good in all the GTIs (second line in Table 3). The best fit N_H was slightly larger than but consistent with the Galactic except in GTI 4, again similar to the results above. In these models the range of the ionization parameter is $3 < U < 28$ and the column density of the warm absorber is $N_H=0.4\text{--}3.2 \times 10^{22} \text{ cm}^{-2}$, consistent with

the results of the empirical fits.

3.1. Variability

As mentioned previously, the flux level of NGC3516 is variable as a function of time (Figure 1). However, the variability of opacities in OVII and OVIII absorption edges is not significant (Figure 1, $\lesssim 2\sigma$ variations). So all the GTIs were fitted together, leaving relative normalization free, resulting in a tighter constraint on U ($6 \lesssim U \lesssim 13$, 90% confidence). If the entire data set is fitted (i.e. without dividing into separate GTIs), then the range in U is even smaller ($7.9 \lesssim U \lesssim 12.6$, 90% confidence) and $N_H = 0.7 \pm 0.1 \times 10^{22} \text{ cm}^{-2}$ (Table 3). We use these values of U and N_H in the rest of the paper.

The ionization parameter is expected to increase with increasing flux on the photoionization time scale. The OVII photoionization time scale is $t_{ph} = 2 \times 10^5 n_6^{-1}$ seconds (see e.g. Reynolds *et al.* 1995). The lack of variability in OVII the opacity implies that $t_{ph} \gtrsim 10^4$ seconds. This puts an upper limit on the density of the absorber, $n \lesssim 2 \times 10^7 \text{ cm}^{-3}$.

In the UV, variations of absorption line strengths on timescales of days have been discussed for the CIV absorber and used to derive a density of $n \gtrsim 10^5 \text{ cm}^{-3}$ in the absorbing region (Voit *et al.* 1987). This calculation, however, assumes that CIV is the dominant ionization state. In the present case, a correction factor of n_{CIV}/n_{CV} needs to be applied to the recombination time scale. The resulting lower limit on the density of the absorber is then smaller, $n \gtrsim 10^3 \text{ cm}^{-3}$.

4. Comparison with the *Ginga* results

The power-law slope in the ROSAT PSPC data is much steeper ($\alpha \sim 1$) than that seen by *Ginga* ($0.25 < \alpha < 0.43$, KEA). Since the PSPC range is dominated by the absorber, the *Ginga* slope is more likely to indicate the true power-law slope. The ROSAT PSPC data show no significant excess cold absorption, but require a warm absorber with $N_H \sim 7 \times 10^{21} \text{ cm}^{-2}$ and $8 \lesssim U \lesssim 13$. It can be seen from Figure 5 that this model does *not* predict the presence of an Fe edge ($\tau_{pred} \lesssim 0.025$). This is inconsistent with the *Ginga* data

which showed a “cold” absorber ($N_{\text{H}} \sim 10^{22} \text{ cm}^{-2}$) and an Fe edge. As can be seen in Figure 5, the ionized absorber causes a low energy turn-over within the *Ginga* band which would mimic “cold absorption” in the *Ginga* data. Indeed, re-analysis of the *Ginga* data showed that the low energy turn-over is most likely due to the warm component (Nandra & Pounds 1994). However, the origin of the Fe-K edge would have to be different from the XUV absorber discussed here. It may be, e.g., from the torus (Krolik and Kriss 1995) which possibly grazes our line of sight. Alternatively, the Fe edge and the large column may be associated with an absorption system that has moved out of the line of sight. We note in passing that there is no obvious Fe edge in recent ASCA observations (Kriss *et al.* 1996a).

5. Comparison of X-ray and UV absorbers

In many AGN, the X-ray and UV absorbers have been found to be one and the same (the ‘XUV Absorbers’: Mathur *et al.* 1994, 1995). In these cases apparent inconsistencies between the conditions in the UV and X-ray were resolved by realizing that the ions observed in the UV were not the dominant ions in the gas. NGC 3516 also shows both X-ray and UV absorbers. In a previous study based on the simultaneous (October 1989) *Ginga* and IUE observations, KEA concluded that, if an X-ray ionized absorber is present, it is unlikely to be due to the same gas as the UV absorber. The combination of the strength of the UV CIV absorption and the very high ionization state of Fe ($\gtrsim 12$, consistent with $> 5\times$ ionized C) indicated by the ionized absorber model fit to the *Ginga* data implied to the authors that a consistent solution was unlikely, although no detailed calculations were presented. Since the ionized absorber observed with ROSAT is clearly different from the *Ginga* absorber, the question of an XUV absorber in NGC3516 should be revisited.

Here we investigate quantitatively whether the ROSAT ionized absorber is consistent with the broad UV absorber with high ionization lines. We use the method described in Mathur *et al.* (1995). The ROSAT observations were made in 1992. There were no simultaneous UV observations. The 1993 IUE observations show that the broad UV high ionization absorption lines had disappeared (Koratkar *et al.* 1996). Figure 4 shows the model with fractional ionization of CIV as a function of U. If the ionization parameter of the X-ray absorber were toward the high end of the observed range (U=12.8), the ionization fractions of CIV and NV would be very small ($\log f \lesssim -4$). Assuming solar abundances of carbon and nitrogen (3.63×10^{-4} and 1.12×10^{-4} respectively, Grevesse & Andres 1989)

and the total column density of $7 \times 10^{21} \text{ cm}^{-2}$ as derived from the X-ray data gives $N(\text{CIV}) < 10^{14} \text{ cm}^{-2}$ and $N(\text{NV}) < 8 \times 10^{13} \text{ cm}^{-2}$. The absorption lines would not be detected. In this case there would be an X-ray ionized absorber, but no broad high ionization UV lines of CIV or NV, consistent with the observations. However, the X-ray absorber must produce a detectable OVI $\lambda 1034$ line with $-2.1 \lesssim \log f_{\text{OVI}} \lesssim -2.7$ (Figure 4). Since there were no contemporaneous far-UV observations with ROSAT, this cannot be directly tested. Analysis of absorption lines embedded in the emission line profiles of quasars is extremely difficult since the shape of the emission lines is unknown. However, visual inspection of the 1995 HUT data for NGC3516 (Kriss et al 1996b) shows a broad absorption feature blue-wards of the OVI emission line peak and at roughly the expected redshift of the broad UV absorber.

It is also of interest to point out the position of the broad CIV and NV absorption lines on the f-U curve when they were strong. The equivalent width of the variable broad CIV absorption line in the IUE observations ranged from $\sim 3\text{\AA}$ to $\sim 10\text{\AA}$ (KEA) leading to a lower limit on the CIV column density $N_{\text{CIV}} > 2.2 \times 10^{15} \text{ cm}^{-2}$. Similarly Voit *et al.* (1987) report $N_{\text{CIV}} \gtrsim 10^{15} \text{ cm}^{-2}$. Assuming this lower limit gives a lower limit on the ionization fraction of CIV: $f_{\text{CIV}} \gtrsim 4 \times 10^{-4}$ ($\log f_{\text{CIV}} \gtrsim -3.4$). The NV EW given by KEA varies in the range 1.1 – 7.1 \AA . This corresponds to $N(\text{NV}) > 3.5 \times 10^{14} \text{ cm}^{-2}$ (using oscillator strength $f=0.235$, Allen 1973). The lower limit on the ionization fraction of NV is estimated to be $f_{\text{NV}} \gtrsim 5 \times 10^{-4}$ ($\log f_{\text{NV}} \gtrsim -3.3$). The arrows in Figure 4 indicate these lower limits on f_{CIV} and f_{NV} observed by IUE. These lie in a range of U smaller than that corresponding to the ROSAT observations. This suggests that if U increases as a function of time, both the former presence and current absence of the broad UV lines would be consistent with the observed X-ray warm absorber.

The IUE data have occasionally shown the presence of a noisy, possibly broad SiIV absorption feature (Voit, Shull & Begelman 1987). The conditions of the warm absorber derived here do not predict detectable SiIV absorption ($\log f_{\text{SiIV}} \lesssim -30$). However, SiIV absorption is also present, with no significant change in strength, in the 1993 IUE spectra in which no broad, high ionization lines are reported (Koratkar *et al.* 1996). Thus it appears that the feature is a part of the narrow UV absorption system rather than the XUV absorber. Note that the two other objects with well-studied XUV absorbers (e.g. 3C351, NGC5548) do not have any such additional narrow absorption systems. It is possible that the second, low column density absorber observed in the ROSAT data is related to this narrow UV system.

6. Discussion

We argue that NGC3516 contains an XUV absorber. It has high column density ($N_H = 7 \pm 1 \times 10^{21} \text{ cm}^{-2}$) derived from the X-ray observations. The UV observations imply that the absorber is outflowing with a velocity of $\sim 500 \text{ km s}^{-1}$ (given its blueshift) and the line width implies an internal velocity dispersion of $< 2000 \text{ km s}^{-1}$ (see sec. 1). Assuming the upper limit on its ionization parameter ($U < 13$), a density of $2 \times 10^5 \text{ cm}^{-3}$, and $N_H = 7 \times 10^{21} \text{ cm}^{-2}$, the distance of the absorber from the central continuum source is $< 5 \times 10^{18} \text{ cm}$ and its thickness is about $3.5 \times 10^{15} \text{ cm}$. At this high value of U no detectable broad UV lines are predicted (sec. 3, fig. 4), consistent with the disappearance of the broad UV absorption lines (Koratkar *et al.* 1996, Kriss *et al.* 1996b).

Kriss *et al.* (1996b) have presented higher resolution ASCA data of the ionized absorber in NGC3516. Based on the non-detection of X-ray absorption lines in the ASCA data they have argued that the velocity dispersion parameter ‘b’ of the absorber is not larger than $\sim 200 \text{ km s}^{-1}$. This result is based on the models of Krolik & Kriss (1995) in which resonance line scattering is an important process. In this case the X-ray absorber is narrow while the UV absorber is broad, implying that the two cannot originate in the same gas. We note however that their models covered the b range from 10 km s^{-1} to 200 km s^{-1} , and did not definitively rule out the presence of broad ($\sim 2000 \text{ km s}^{-1}$) blended features which could mimic a different continuum shape. More importantly, in similar models presented by Netzer (1996), absorption and emission due to resonance line scattering almost identically cancel out so that no absorption lines are expected even for turbulences significantly larger than the thermal line widths. Thus, the non-detection of absorption lines in ASCA data may simply be because there are no lines there. Clearly the theoretical situation is too uncertain for the absence of features to provide constraints on the b parameter of the absorbing gas. Since the UV absorber has a measured width of $\sim 2000 \text{ km s}^{-1}$, we will adopt this value in our ensuing discussion of a combined X-ray/UV absorbing region.

We have seen that the X-ray absorber is consistent with both the presence of the broad UV absorption lines in the past and their subsequent absence, but can we develop a consistent physical picture to explain this variation? The evolution of ionization parameter as seen in figure 4 is suggestive. The earliest known observations of the broad UV absorption lines are from 1978. Strong lines were also observed in 1989 (KEA), while they have disappeared since ~ 1993 . Thus the large scale variability time scale of the absorber seems to be some 3–6 years. Given its outflow velocity, the distance traveled by the absorber away from the ionizing continuum source in this time is $5 \times 10^{15} \text{ cm}$. Clearly, this is a small

fraction of the distance of the absorber from the central continuum and there would be no significant change in ionization parameter corresponding to this change in flux. On the other hand, the velocity dispersion of the absorber is large ($\text{FWHM} \sim 2000 \text{ km s}^{-1}$). If the absorber is expanding at this rate, its thickness will change by $\sim 2 - 4 \times 10^{16} \text{ cm}$ in 3–6 years. Thus, to have a present thickness of $\sim 3.5 \times 10^{16} \text{ cm}$, the thickness of the absorber 3 years ago must have been $\lesssim 1.5 \times 10^{16} \text{ cm}$ with a corresponding density of $\gtrsim 5 \times 10^5 \text{ cm}^{-3}$. Then the ionization parameter in the past could be as low as $U=5$, (see fig. 4) where the strength of the broad UV absorption lines would be in the observed IUE range. CIV and NV lines would then be strong. In this scenario the disappearance of the broad UV absorption lines is due to increase in U caused by the drop in the density of the absorber as it expands while outflowing from the ionizing source. For this scenario to work, the fractional change in the thickness of the absorber in 3–6 years should be significant. If the absorber is dispersed in velocity space, the ‘b’ parameter of each cloud would be smaller. If we consider a conservative estimate of $\sim 200 \text{ km s}^{-1}$ of the velocity dispersion, a significant change in the thickness of the absorber would require a density in the higher end of the allowed range ($n \gtrsim 10^6 \text{ cm}^{-3}$).

The XUV absorber picture is thus completely consistent with the observations: the presence of X-ray absorption edges, the presence of broad absorption lines in the old IUE spectra and their disappearance in the the new UV observations. In this scenario the broad UV absorption lines will not reappear unless a new, similar absorption system is generated. Over the next ~ 15 years the current absorber will become more highly ionized, the OVI absorption lines will disappear, and the OVIII edge will become stronger than the OVII edge. Eventually, it will be completely transparent in X-rays and the OVII/OVIII edges will disappear. This is an easily testable prediction with future missions. These estimates of time scale and the amount of change in U are based on assuming $b=2000 \text{ km s}^{-1}$ and density of $\sim 2 \times 10^5 \text{ cm}^{-3}$. If the internal velocity dispersion is smaller, the evolution described above would be slower. We note that this picture concerns long term variations, we expect in addition small scale variations due to flux variability.

As noted earlier, new simultaneous HUT (UV) and ASCA (X-ray) observations are presented by Kriss *et al.* (1996a,b). These data show an X-ray ionized absorber similar to that reported here and narrow, associated absorption lines in the UV. The authors are unable to reconcile the X-ray and UV absorbers with a single absorbing region. This is entirely consistent with our model predictions in which the X-ray warm absorber is instead associated with the now invisible broad UV absorption. The absorption systems in NGC3516 are clearly complex and multiple. The Kriss *et al.* (1996a,b) study shows

that each of the X-ray and narrow UV absorbers require at least two separate systems to match the data. More, simultaneous X-ray and UV data allowing monitoring of the various components is necessary to disentangle them. We cannot rule out the possibility that the X-ray and UV absorbers are different. In that case the disappearance of the broad absorption lines may be due to the clouds moving out of line of sight as suggested by Walter *et al.* (1990). Our XUV absorption scenario offers an alternative explanation.

An edge-on orientation of 3C351, 3C212 and NGC5548 was inferred from their lobe dominated radio structure. NGC3516 also has a steep radio spectrum (Ulvastad and Wilson 1989) typical of lobe dominated AGN. Its radio maps reveal an elongated, one sided, curved structure (Miyaji *et al.* 1992). The geometrical structure of NGC3516 was inferred by Goad and Gallagher (1987) by analyzing the velocity field of the circumnuclear emission-line region. They found a bipolar outflow from the nucleus in the plane of the sky so that our line of sight grazes the putative torus. Thus to date all active galactic nuclei shown to contain XUV absorbers are edge on, consistent with the picture of outflowing absorbers suggested by Glen, Schmidt, & Foltz (1994).

7. Conclusions

ROSAT observations of NGC3516 in 1992 detected an X-ray warm absorber with $N_{\text{H}} \sim 7 \times 10^{21} \text{ cm}^{-2}$ and $U \sim 7.9\text{--}12.6$. Combining X-ray and UV observations imply that it is outflowing with a velocity of $\sim 500 \text{ km s}^{-1}$ and has an internal velocity dispersion of $\lesssim 2000 \text{ km s}^{-1}$. The constraints on density are not very tight: $10^3 \lesssim n \lesssim 10^7 \text{ cm}^{-3}$. The distance of the absorber from the central continuum source is $\lesssim 5 \times 10^{18} \text{ cm}$ and its thickness is about $3.5 \times 10^{15} \text{ cm}$ assuming density of $2 \times 10^5 \text{ cm}^{-3}$. The physical characteristics of the absorber are consistent with all the observations: the presence of X-ray absorption edges, the presence of broad absorption lines in the old IUE spectra and their disappearance in the the new UV observations. In this scenario of the XUV absorber in NGC3516, the disappearance of the broad UV absorption lines is due to the current high value of U caused by the drop in the density of the absorber as it expands and moves away from the ionizing source. If this dynamical model is correct, we expect the OVII absorption edge in the X-rays to weaken compared to the OVIII edge. Eventually the source would be transparent to the X-rays as the absorber continues to expand, unless a new absorption system is produced.

Acknowledgements: It is our pleasure to thank our colleagues Martin Elvis and Paul O’Brien for useful discussions. The financial support of the following NASA contracts and grants is gratefully acknowledged: NAGW-4490 (LTSA), NAS5-30934 (RSDC), NAS8-39073 (ASC).

REFERENCES

- Allen, C. W. 1973, *Astrophysical Quantities* [The Athlone]
- Ferland, G. F. 1991 “HAZY”, OSU Astronomy Department Internal Report
- Fiore, F., Elvis, M., Mathur, S., Wilkes, B., & McDowell, J. 1993, *ApJ*, 415, 129
- Glenn, J., Schmidt, G., & Foltz, C. 1994, *ApJL*, 434, L47
- Grevesse, N., & Andres, E. 1989 in *Cosmic Abundances of Matter*, AIP Conference Proceedings, 183, 1. Ed. C. J. Waddington (New York: AIP)
- Halpern, J. 1982, Ph. D. Thesis, Harvard University
- Heiles, C. 1975, *A&A*, 20, 37
- Kriss, G. *et al.* 1996a *ApJL in press*
- Kriss, G., Espey, B.R., Krolik, J.H., Tsvetanov, Z., Zheng, W. and Davidsen, A.F. 1996b *ApJL in press*
- Krolik, J. & Kriss, G. 1995, *ApJ*, 447, 512
- Koratkar, A. *et al.* 1996, *ApJ in press*
- Kolman, M., Halpern, J. P., Martin, C., Awaki, H. & Koyama, K. 1993, *ApJ*, 403, 592 (KEA)
- Mathur, S. 1994 *ApJL*, 431, L75
- Mathur, S., Wilkes, B. J., Elvis, M. S., & Fiore, F. 1994 *ApJ*, 434, 493
- Mathur, S., Elvis, M. S. & Wilkes, B. J. 1995, *ApJ*, 452, 230
- Nandra, K. & Pounds, K. A. 1994, *M.N.R.A.S.*, 268, 405
- Netzer, H. 1996 Preprint.
- Morrison, R. & McCammon, D. 1983 *ApJ* 270, 119

- Pfeffermann, E., Briel, U. G., Hippmann, H., Kettenring, G., Metzner, G., Predehl, P., Reger, G., Stephan, K.-K., Zombeck, M. V., Chapell, J. & Murray, S. S. 1987 Proc. SPIE Int. Soc. Eng. 733, 519
- Reynolds, C. & Fabian, A. 1995, MNRAS, 273, 1167
- Shull, J.M., & van Steenburg, M. 1982 ApJS 48, 95
- Turner, T. J., Nandra, K., George, I. M., Fabian, A., & Pounds, K. A. 1994, ApJ, 419, 127
- Trümper, J. 1983, Adv. Space Res., 2, No. 4, 241
- Ulrich, M. H. & Boisson, C. 1983, ApJ, 267, 515
- Voit, G. M., Shull, J. M. & Begelman, M. C. 1987, ApJ, 316, 573
- Walter, R., Ulrich, M. H., Courvoisier, T. J. L. & Buson, L. M. 1990, A&A, 233, 53

Figure 1: NGC 3561 light curve (top panel), τ_{OVII} (middle panel), τ_{OVIII} (bottom panel), for the eight GTIs.

Figure 2: Residuals to the simple power-law fit to the entire data. The strong negative residuals between 0.7 and 1 keV are clearly visible. Channels 13–25 corresponding to this energy range were ignored in the PL fit to show the absorption edges clearly.

Figure 3: Data and the best fit spectrum (PL+2 Edges, N_H fixed to Galactic).

Figure 4: Ionization fractions f of OVI, OVII, OVIII, CIV and NV as a function of ionization parameter, U . The vertical lines define the range of U for which the ratio f_{OVII}/f_{OVIII} lies within the observed range. The arrows on the CIV and NV curves indicate the lower limits of $f_{CIV} \gtrsim 3 \times 10^{-4}$ and $f_{NV} \gtrsim 3.1 \times 10^{-4}$ based on the published IUE data (see text).

Figure 5: The input spectrum (solid line) and the transmitted spectrum (dotted line) for $N_H = 10^{22} \text{ cm}^{-2}$ and $U=10$. The transmitted spectrum shows strong OVII/OVIII edges, but no Fe-K edge or low energy cutoff.

Table 1: ROSAT Observations of NGC 3516

Observation	Net Counts	Exposure (s)	Net Count Rate (s ⁻¹)
Total	59225±246	13081	4.53±0.02
GTI 1	12860±127	3176	4.05±0.04
GTI 2	4186±69	1150	3.64±0.06
GTI 3	4068±71	1014	4.01±0.07
GTI 4	14848±116	2900	5.12±0.04
GTI 5	7007±96	1375	5.10±0.07
GTI 6	7670±97	1612	4.76±0.06
GTI 7	1027±39	232	4.43±0.17
GTI 8	7571±97	1622	4.67±0.06

Table 2: Spectral fits to ROSAT data of NGC 3516

Data	Model	α_E	Normalization ^a	τ_{OVII}	τ_{OVIII}	χ^2 (dof)	F ^b
GTI 1 ^c	PL	1.22±0.01	1.36±0.01			132.2 (30)	
	PL+ 1Edge	1.07±0.03	1.70±0.07	0.8±0.15		43.55 (29)	59.0
	PL+ 2Edges	1.04±0.035	1.76±0.07	0.46 ^{+0.19} _{-0.17}	0.45±0.19	31.11 (28)	11.2
GTI 2	PL	1.18±0.04	1.24±0.04			56.5 (30)	
	PL+ 1Edge	1.06±0.06	1.51±0.11	0.71 ^{+0.27} _{-0.26}		33.68 (29)	19.6
	PL+ 2Edges	1.05±0.06	1.53±0.12	0.62±0.35	0.11 ^{+0.36} _{-0.11}	33.45 (28)	0.2
GTI 3 ^c	PL	1.23±0.03	1.33±0.03			62.87 (30)	
	PL+ 1Edge	1.08±0.06	1.69±0.13	0.9±0.3		32.17 (29)	27.7
	PL+ 2Edges	1.02±0.07	1.8±0.14	0.34±0.33	0.75 ^{+0.35} _{-0.37}	22.00 (28)	12.9
GTI 4 ^c	PL	1.26±0.01	1.69±0.02			154.1 (30)	
	PL+ 1Edge	1.12±0.02	2.08±0.05	0.77±0.08		59.57 (29)	46.0
	PL+ 2Edges	1.09±0.03	2.16±0.09	0.43 ^{+0.18} _{-0.16}	0.45±0.18	44.87 (28)	9.2
	Best Fit ^d	1.24±0.09	2.23±0.09	0.75 ^{+0.29} _{-0.25}	0.19 ^{+0.24} _{-0.19}	34.55 (27)	8.1
GTI 5	PL	1.22±0.02	1.72±0.08			66.20 (30)	
	PL+ 1Edge	1.09±0.04	2.09±0.11	0.72 ^{+0.20} _{-0.19}		25.16 (29)	47.3
	PL+ 2Edges	1.08±0.05	2.13±0.13	0.57 ^{+0.30} _{-0.25}	0.20 ^{+0.28} _{-0.20}	23.91 (28)	1.5
GTI 6	PL	1.16±0.02	1.55±0.03			117.4 (30)	
	PL+ 1Edge	1.07±0.04	2.1±0.1	1.1±0.2		20.89 (29)	134.0
	PL+ 2Edges	1.06±0.04	2.1±0.1	1.0±0.3	0.06 ^{+0.3} _{-0.06}	20.81 (28)	0.1

Table 2: Continued.

GTI 7	PL	1.2 ± 0.1	1.5 ± 0.1			19.91 (30)	
	PL+ 1Edge	1.0 ± 0.13	2.0 ± 0.3	$1.0^{+0.7}_{-0.6}$		11.83 (29)	19.8
	PL+ 2Edges	1.0 ± 0.1	1.99 ± 0.35	$0.73^{+0.36}_{-0.68}$	$0.3^{+0.8}_{-0.3}$	11.5 (28)	0.8
GTI 8 ^c	PL	1.19 ± 0.02	1.60 ± 0.03			71.16 (30)	
	PL+ 1Edge	1.06 ± 0.04	1.9 ± 0.1	0.7 ± 0.2		29.08 (29)	42.0
	PL+ 2Edges	1.03 ± 0.05	2.01 ± 0.11	$0.4^{+0.25}_{-0.22}$	$0.4^{+0.26}_{-0.27}$	22.74 (28)	7.8
GTI 1-8	PL+ 2Edges	1.06 ± 0.02		0.53 ± 0.09	0.37 ± 0.09	244.6 (245)	
	PL+ 2Edges (N_H free)	1.16 ± 0.04		$0.74^{+0.15}_{-0.13}$	$0.19^{+0.12}_{-0.13}$	226.9 (244)	

a: in units of 10^{-2} photons $\text{keV}^{-1} \text{cm}^{-2} \text{s}^{-1}$ at 1 keV

b: Parameter of the F-test. Note that $F \gtrsim 7.5$ is 99% significant and $F \gtrsim 13$ is 99.9% significant

c: datasets for which two edges are required by the data

d: PL+ 2Edges+ Excess absorption at the source (see text).

Table 3: Warm absorber model fits to ROSAT data of NGC 3516

Data	α_E	Normalization ^a	N_H^b (warm)	$\log U$	χ^2 (dof)
GTI 1	$0.91^{+0.06}_{-0.08}$	$2.15^{+0.23}_{-0.17}$	$1.26^{+0.34}_{-0.42}$	$1.34^{+0.07}_{-0.12}$	37.02 (28)
	$1.1^{+0.2}_{-0.1}$	$2.22^{+0.15}_{-0.17}$	$0.77^{+0.42}_{-0.28}$	$1.09^{+0.2}_{-0.25}$	30.41 (27)
GTI 2	0.95 ± 0.11	$1.79^{+0.28}_{-0.22}$	0.69 ± 0.37	$1.16^{+0.23}_{-0.44}$	32.56 (28)
	1.4 ± 0.3	$2.2^{+0.6}_{-0.4}$	$0.4^{+0.2}_{-0.1}$	$0.45^{+0.57}_{-0.45}$	26.41 (27)
GTI 3	0.82 ± 0.65	$2.37^{+0.48}_{-0.03}$	3.19 ± 0.85	$1.49^{+0.01}_{-0.03}$	23.80 (28)
	$0.82^{+0.3}_{-0.2}$	$2.41^{+0.5}_{-0.2}$	$3.35^{+0.79}_{-3.34}$	$1.49^{+0.008}_{-0.65}$	23.52 (27)
GTI 4	$0.9^{+0.5}_{-0.1}$	2.76 ± 0.12	$2.1^{+1.2}_{-2.05}$	$1.46^{+0.03}_{-0.04}$	50.72 (28)
	$1.3^{+0.3}_{-0.1}$	$2.9^{+0.5}_{-0.2}$	$0.6^{+0.3}_{-0.2}$	$0.9^{+0.2}_{-0.5}$	31.54 (27)
GTI 5	0.94 ± 0.56	$2.59^{+0.58}_{-2.56}$	$1.2^{+1.4}_{-1.2}$	$1.34^{+0.15}_{-0.20}$	26.94 (28)
	$1.3^{+0.5}_{-0.2}$	$2.81^{+0.9}_{-0.3}$	$0.5^{+0.4}_{-0.1}$	$0.81^{+0.3}_{-0.8}$	17.35 (27)
GTI 6	0.95 ± 0.48	2.54 ± 0.09	$0.90^{+0.5}_{-0.89}$	$1.14^{+0.19}_{-0.18}$	32.00 (28)
	$1.3^{+0.7}_{-0.2}$	$2.9^{+1.6}_{-0.3}$	$0.6^{+0.3}_{-0.2}$	$0.8^{+0.3}_{-0.8}$	21.45 (27)
GTI 7	$0.87^{+0.36}_{-0.25}$	$2.44^{+0.99}_{-0.64}$	$1.03^{+2.24}_{-1.0}$	$1.22^{+0.27}_{-1.22}$	11.98 (28)
	$1.0^{+1.1}_{-0.7}$	$2.5^{+2.5}_{-0.7}$	$0.8^{+2.9}_{-0.7}$	$1.06^{+0.4}_{-1.06}$	11.77 (27)
GTI 8	0.86 ± 0.49	2.57 ± 0.43	$1.93^{+1.71}_{-1.92}$	$1.45^{+0.04}_{-0.1}$	20.71 (28)
	$1.1^{+0.2}_{-0.3}$	$2.6^{+0.2}_{-0.3}$	$0.8^{+1.6}_{-0.4}$	$1.1^{+0.3}_{-0.4}$	19.05 (27)
Total	1.21 ± 0.06	$2.54^{+0.1}_{-0.08}$	0.7 ± 0.1	1.0 ± 0.1	28.01 (27)

a: in units of 10^{-2} photons $\text{keV}^{-1} \text{cm}^{-2} \text{s}^{-1}$ at 1 keV

b: in units of 10^{22} atoms cm^{-2}

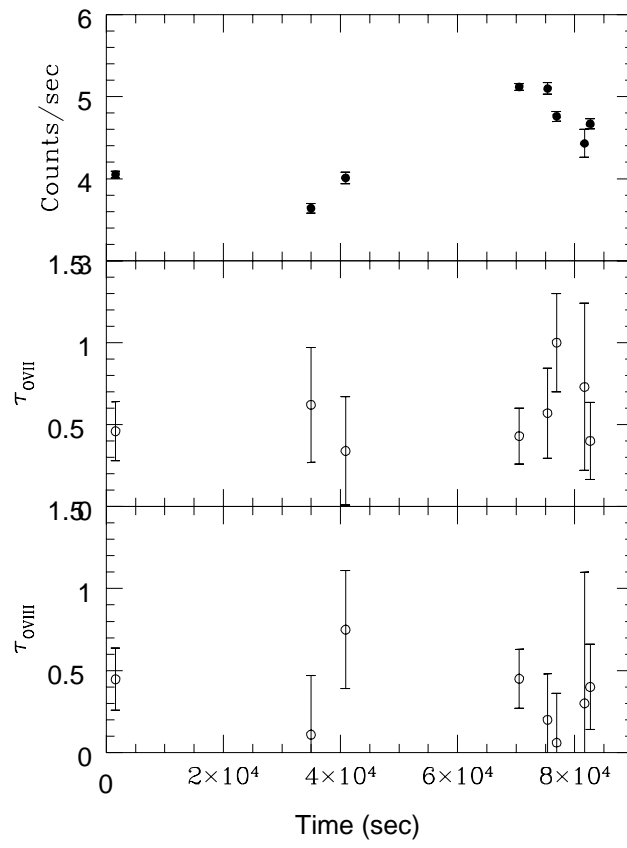


Fig. 1.—

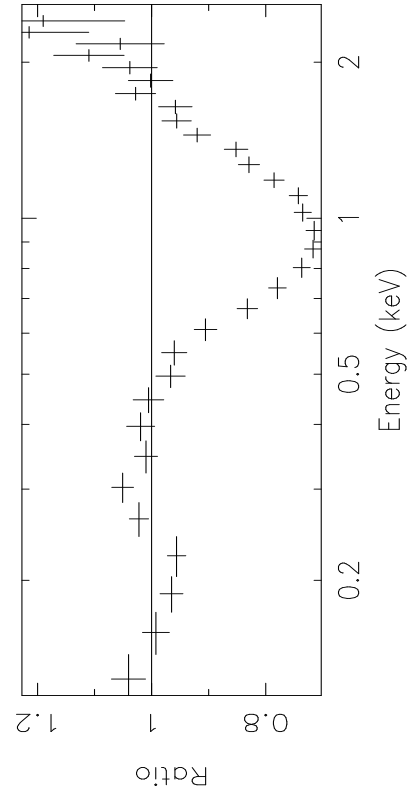


Fig. 2.—

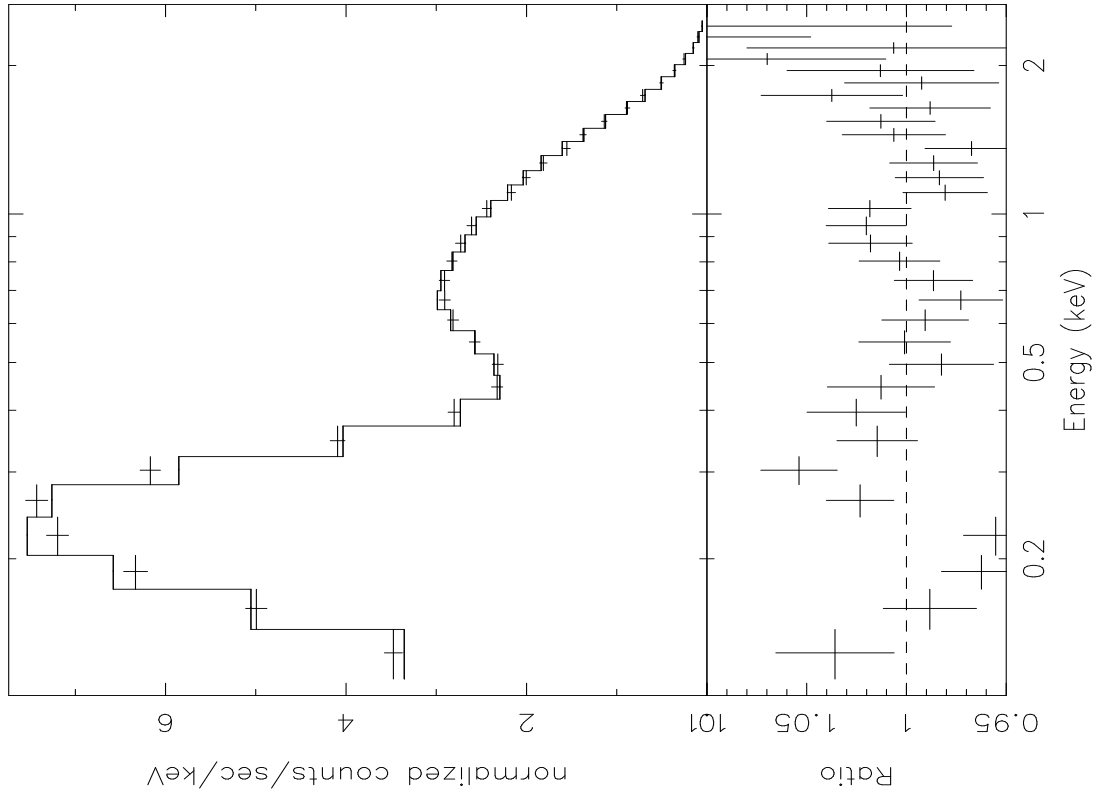


Fig. 3.—

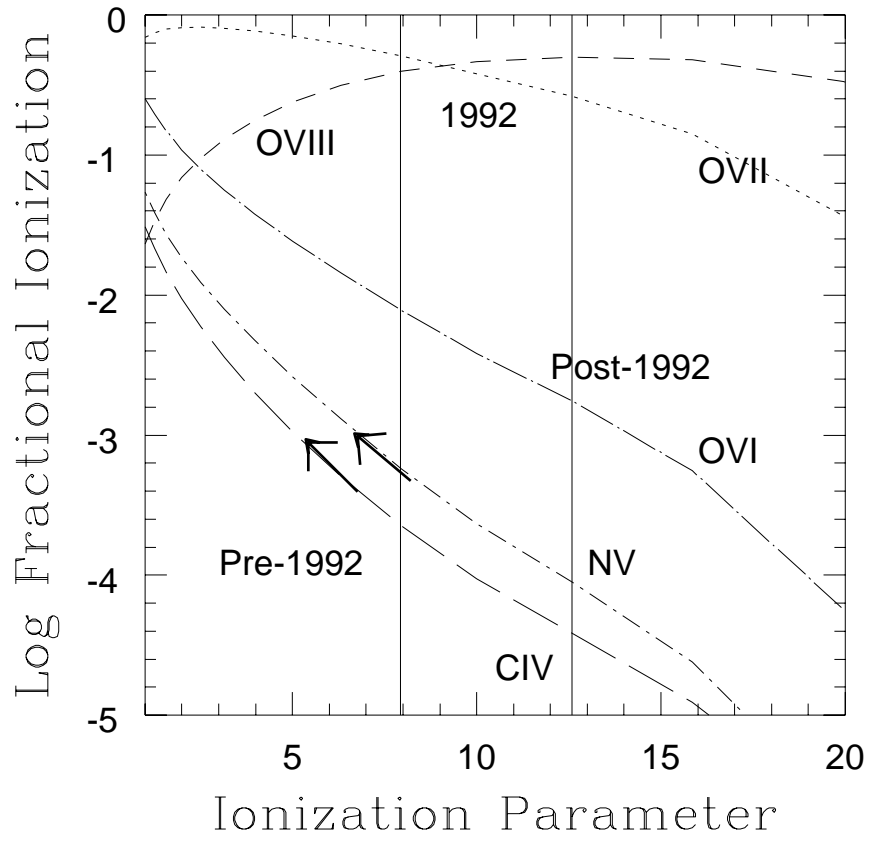


Fig. 4.—

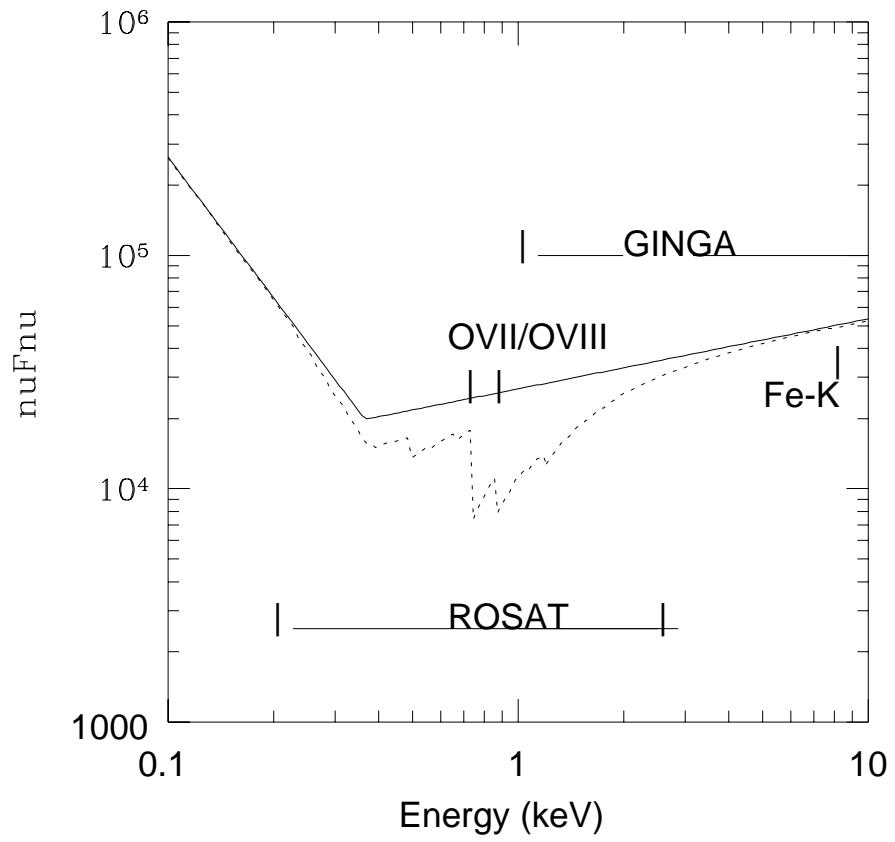


Fig. 5.—